Atmospheric Environment 311 (2023) 119995

Contents lists available at ScienceDirect

Atmospheric Environment

journal homepage: www.elsevier.com/locate/atmosenv

Towards hyperlocal source identification of pollutants in cities by combining mobile measurements with atmospheric modeling

John C. Lin [a,*], Ben Fasoli [a], Logan Mitchell [a,1], Ryan Bares [a,2], Francesca Hopkins [b], Tammy M. Thompson [c], Ramón A. Alvarez [c]

[a] Department of Atmospheric Sciences, University of Utah United States
[b] Dept. of Environmental Sciences, University of California, Riverside United States
[c] Environmental Defense Fund United States

HIGHLIGHTS

- Mobile vehicle monitoring reveals pollution patterns in Salt Lake City.
- Minorities and lower income groups are exposed to higher pollution levels.
- Mobile monitoring, combined with atmospheric modeling, can identify pollution source location.
- Pollution source can be localized at high resolution even if not known a priori.

GRAPHICAL ABSTRACT

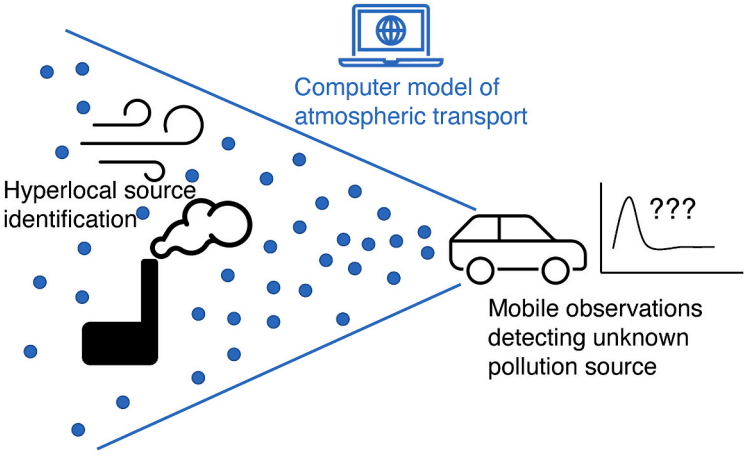

ARTICLE INFO

Keywords:
Urban air quality
Mobile pollution sampling
Atmospheric modeling
Source localization

ABSTRACT

While mobile, vehicle-based sampling of air quality has provided insights into pollutant distributions within cities, previous research has been limited in using observed pollution hotspots to identify and localize unknown emission sources away from the road. Such "hyperlocal source identification" requires hotspots identified through mobile sampling to be linked to emission sources by tracing atmospheric transport upwind from observed hotspots. Here we analyze almost one year's worth of pollutant observations from two Google Street View cars driven around the Salt Lake area, with repeated sampling in select neighborhoods. We then present a method to bridge the gap in hyperlocal source identification by using a high-resolution atmospheric transport model, as part of a new Stochastic Lagrangian Monte Carlo (SLMC) method to identify emission sources based on mobile observations. Case studies with both known and unknown sources are presented to illustrate the efficacy

* Corresponding author.
E-mail address: John.Lin@utah.edu (J.C. Lin).
[1] Current affiliation: Utah Clean Energy.
[2] Current affiliation: Utah Department of Environmental Quality.

https://doi.org/10.1016/j.atmosenv.2023.119995
Received 30 May 2023; Received in revised form 27 July 2023; Accepted 1 August 2023
Available online 2 August 2023

of the SLMC method in hyperlocal source identification. With the availability of techniques like SLMC, we envision mobile air quality monitoring vehicles can serve as "roving sentinels" in identifying unknown pollution sources.

1. Introduction

By the beginning of the 21st century, more than half of humanity reside in cities (Seto et al., 2012), where large numbers of people are living in close proximity to pollutant emissions. Thus urban air pollution is a significant health risk for millions of people worldwide (Cohen et al., 2017; Dockery et al., 1993; Hoek et al., 2013; Pope, 2000).

Since the 1970s, air pollution in cities has primarily been monitored using stationary instruments, especially under regulatory frameworks such as the U.S. Clean Air Act. Among pollutants regulated under the Clean Air Act are fine particulate matter ($PM_{2.5}$) and nitrogen dioxide (NO_2). However, distributions of such pollutants within urban areas have been found to be highly variable, with fine-scale exposure patterns (Alexeeff et al., 2018; Fruin et al., 2014; Kaur et al., 2007) related to differences in traffic, street canyon morphology, and distance to emission sources (Van den Bossche et al., 2015). The considerable spatiotemporal variation of pollution in cities means that stationary sensors may not properly characterize the variability of pollutants and human exposure (Alexeeff et al., 2018; Kaur et al., 2007; Van den Bossche et al., 2015).

In recent years, developments in sensor design and communications technologies have facilitated novel methods to monitor pollution at finer granularity. Lower cost sensors that enable much larger numbers of sites to be placed around a city have begun to fill spatial gaps in the pollution picture (Caubel et al., 2019; Delaria et al., 202; Feenstra et al., 2019; Morawska et al., 2018).

Alternatively, mobile observations address the sampling gaps by placing instruments on platforms that move across the urban landscape. Air pollution monitoring using instrumented vehicles can sample wherever the vehicle can be driven, and mobile sampling using instrumented vehicles has yielded significant insights into urban pollution patterns. In particular, vehicle-based mobile sampling has been invaluable for identifying urban hotspots around the city for pollutants such as black carbon (BC), NO_2, and fine particulates (Apte et al., 2017; Deshmukh et al., 2020; Hu et al., 2016; Padilla et al., 2021; Targino et al., 2016). Vehicle-based mobile sampling has also been used to evaluate street-level differences in health impacts such as cardiovascular events due to long-term exposure to NO_2, NO, and BC (Alexeeff et al., 2018). Additionally, mobile sampling provided compelling evidence of widespread leaks in the natural gas infrastructure that emit methane (CH_4), a potent greenhouse gas, to the atmosphere (Jackson et al., 2014; von Fischer et al., 2017; Weller et al., 2020).

Mobile sampling has also been used to apportion pollutant concentrations to source sectors. For example, analyses of mobile data using Positive Matrix Factorization modeling (PMF) can quantify the relative contribution of source sectors to fine resolution measurements of $PM_{2.5}$ species, or hydrocarbons (Robinson et al., 2018; Gu et al., 2018) providing insight into the relative importance of source sectors. However, chemical signatures alone cannot determine the location of the source (Shah et al., 2018). Pekney et al. (2006) took PMF a step further and applied the Potential Source Contribution Function (PSCF) methodology using 24-hr averaged measurements along with mean-wind trajectories (neglecting turbulence) to identify likely source regions at the $0.1^\circ \times 0.1^\circ$ (~10 km) grid scale. A key result was to distinguish between local and regional sources, without the capability to localize the source more precisely. Additionally, the equipment required to run chemical speciation profiles on $PM_{2.5}$ requires a sophisticated mobile monitoring set up, thus limiting the scalability of this approach.

While mobile sampling has hitherto contributed to growing understanding of pollutant distribution and hotspots within cities, previous research has been limited in terms of relating such hotspots to their source locations, away from the road, in a quantitative manner. Past work on mobile data has mostly presented the hotspots solely using empirical, statistical methods—e.g., elevated median values (Apte et al., 2017; Miller et al., 2020). Conducting "hyperlocal source identification" requires the hotspots discerned through mobile sampling to be linked to emission sources by tracing the transport of pollutants upwind from the hotspots. Tracing such hotspots upwind to the sources using atmospheric transport information is either missing from previous studies or only carried out in a relatively simple manner—e.g., using wind categories based on limited weather station data (Brantley et al., 2019; Deshmukh et al., 2020) or using mean-wind trajectories, without accounting for turbulence, in the case of PSCF (Pekney et al., 2006).

Due to limited usage of wind information, published studies have primarily linked identified hotspots to prominent sources that are already known a priori, such as busy thoroughfares (Padilla et al., 2021), traffic intersections (Apte et al., 2017), rail yards (Brantley et al., 2014a; Deshmukh et al., 2020; Mitchell et al., 2018), or highways (Apte et al., 2017; Deshmukh et al., 2020). The research literature is lacking in ways to identify previously unknown sources away from the road, based on vehicle-based mobile sampling, by accounting for atmospheric transport in a more sophisticated methodology. One of the few notable exceptions is the study by Valencia et al. (2021), which combines mobile sampling with dispersion modeling to adjust prior source emissions from inventories. Although one of the most sophisticated studies to date, the study still relies upon a single meteorological site to drive the dispersion model throughout the city, and the source identification depends on adjusting a prior emission inventory, meaning that missing sources are difficult to be adjusted if entirely absent from the inventory (Hopkins et al., 2016). Therefore, the identification of unknown sources is a current gap in the advancement of inverse modeling methods aimed at improving prior emissions inventories at any scale.

In this study, we present a way to bridge the gap in hyperlocal source identification found in previous mobile sampling studies by combining pollution data collected from Google Street View cars (Apte et al., 2017; Miller et al., 2020) with a high resolution atmospheric model (Lin et al., 2003; Fasoli et al., 2018). We define "hyperlocal" here as 0.002°, which is approximately 200 m. This spatial resolution allows sources within a Census block level (~1 km) to be resolved.

Our objectives in this paper are twofold: 1) Present empirical analyses of a mobile sampling dataset and 2) Introduce a method to identify source regions of the observed pollutants at high spatiotemporal resolution. The mobile data were collected from two Google Street View vehicles driven for nearly one year (May 2019–March 2020) in Salt Lake City, Utah. Similar to previous studies, we start off by empirically characterizing the spatial distributions of pollutants (BC, NO_x, $PM_{2.5}$) and their hotspots throughout our sampling domain. We then couple the observations with the Stochastic Time-Inverted Lagrangian Transport (STILT) model, driven with wind fields from the High Resolution Rapid Refresh (HRRR) model, to identify the source regions of the observed pollutants at high spatiotemporal resolution. We leverage the information from the atmospheric model and introduce a method to identify emission sources based on mobile observations—the Stochastic Lagrangian Monte Carlo (SLMC) method. Case studies are presented in which sources are known versus unknown to illustrate the efficacy of the SLMC method in hyperlocal source identification. Finally, we discuss remaining uncertainties and ways to further make use of mobile data in the future.

We specifically seek to address the following scientific questions:

- *How are pollutants distributed across Salt Lake City, and how do pollution patterns in residential neighborhoods relate to socioeconomic patterns?*
- *By utilizing detailed atmospheric modeling, can on-road hotspots detect and localize non-road emission sources?*

2. Materials and methods

2.1. Drive planning + coverage characteristics

Two Google Street View vehicles were instrumented for air quality measurements (see below), with each vehicle driven on 4–5 days per week (mostly weekdays). Drives began in May 2019 and ended in March 2020. Vehicle schedules were staggered between a morning shift (6am to 2pm LDT) and an afternoon shift (10am to 6pm LDT). These shifts overlapped in the middle of the day to collect the greatest amount of data when atmospheric conditions are the most well mixed.

Daily routes were conducted by driving on every public road within a series of designated polygon-bounded areas selected across the Salt Lake Valley (Fig. 1), with particularly dense sampling in the middle and northern portions of the Salt Lake Valley. We defined 33 polygon regions—roughly with lengthscale of kilometer(s)—using contiguous census block group boundaries that contained 30–50 km of roads within them. Polygons were also chosen to have a range of population, race, and income demographic characteristics as well as being spatially distributed across the city (Figs. S1 and S5). Each vehicle completed 4–6 polygons each day. We aimed to have >30 drive days in each polygon to determine statistically robust mean concentrations (Fig. S6). On average, 36 drives were conducted in each polygon, roughly even distribution of revisits between the polygons but with slightly more drives occurring during the morning shift compared to the afternoon shift (Fig. S1).

2.2. Vehicles and instrumentation

The two Google Street View vehicles and the associated instruments (Table S1) for NOx, $PM_{2.5}$, BC, and CO_2 are identical to the ones deployed earlier in a previous campaign in Houston, Texas (Miller et al., 2020). Thus, we refer the reader to the Supplement and Miller et al. (2020) for details. Two instruments were added to the vehicles on a temporary basis: a Los Gatos Research Micro-portable greenhouse gas analyzer (GLA131-GGA) yielded CH_4 and redundant CO_2 measurements between June to October 2019, while a Picarro G2401 also provided CH_4, CO, and redundant CO_2 data in August 2019. Details regarding calibrations, the inlet lag determination, and manual QC can be found in the Supplement.

2.3. Baseline/enhancement decomposition

Signals of emissions from pollution sources manifest themselves as enhancements (C_{ex}) in tracer concentrations (C) above a baseline level C_{base}:

$$C = C_{base} + C_{ex}$$

where C can represent the concentrations of NO, NO_2, BC, $PM_{2.5}$, CO_2, or CH_4. Since NOx is the sum of both NO and NO_2, NOx_{ex} is then calculated as the sum of NO_{ex} and NO_{2ex}.

Similar to several previous studies (Apte et al., 2017; Brantley et al., 2014a; Padilla et al., 2021), we adopted a low-quantile method to identify baseline concentrations C_{base}, from which the observed concentration time series can be subtracted to reveal the hyperlocal emission signal in C_{ex}.

The 1% quantile over a moving time window was selected, similar to a previous study in the Salt Lake area (Bares et al., 2018). A time window of 1 h—looking both forward and backward in time (Fig. S2)—was chosen in this study to remove concentration variations unrelated to hyperlocal emissions, such as diel variations in the baseline due to vertical mixing, changes due to weather systems, or long-range transport of pollutants (e.g. regional wildfire smoke). The decision to use 1 h was informed by our transport modeling results, indicating a timescale of 1 h corresponds to the time for air to travel from the boundary of our model domain to the location of the Google Street View vehicle.

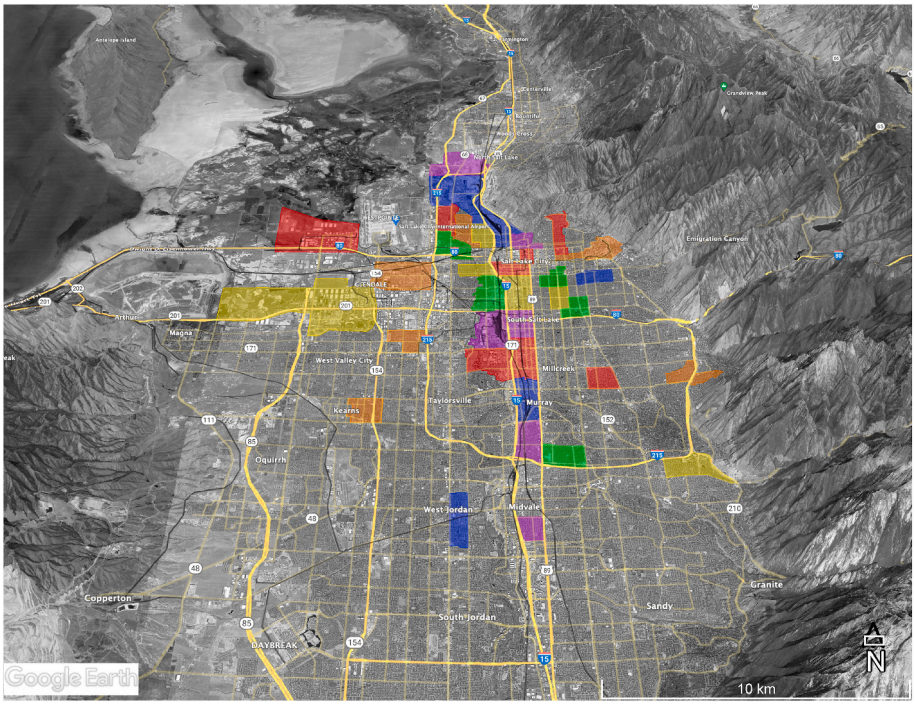

Fig. 1. The study domain over the urban Salt Lake Valley of Utah. The colored polygons are specific areas selected for sampling by the two Google Street View vehicles. Each vehicle sampled 4–6 polygons per day.

2.4. Spatiotemporal aggregation methods

The mobile observations at 1-sec timescale are too variable to reveal spatiotemporal variations in pollutant patterns, calling for suitable averaging or smoothing of the measurements (Brantley et al., 2014b). As such, the mobile observations were aggregated into space/time windows. A "receptor" was created whenever the vehicle covered a distance of 0.002° or when 1 min has elapsed since the previous receptor. For each receptor, the median lat/lon location, tracer concentration, background, and enhancement were recorded. The aggregation resulted in a total of 420,453 receptors for the entire mobile dataset. These receptors serve as the starting locations from where air parcels will be simulated and traced backward in time using the STILT model (Sect. 2.5).

The individual receptors are further aggregated to the 33 target polygon areas used for drive planning (Sect. 2.1). The receptor values are first associated with each polygon, and weighted averaging of the values is carried out per day, with the observation count for the receptor serving as the weights. The vehicle was required to spend a minimum of 1 h in a polygon on a particular day for the data to be included for characterizing polygon-level concentrations. The median of the daily averages within each polygon was further calculated over all observed days to arrive at a single representative value for each polygon. The median was chosen in lieu of the mean to increase robustness to outliers (Brantley et al., 2014a).

2.5. Stochastic Lagrangian Monte Carlo (SLMC) source identification methods

Each of the 420,453 receptors identified using the 0.002°/1 min spatial/temporal window served as the starting point for back-trajectories simulated using the Stochastic Time-Inverted Lagrangian Transport model (STILT) (Lin et al., 2003; Fasoli et al., 2018; Loughner et al., 2021). STILT simulates the three-dimensional trajectories of air parcel ensembles transported backward in time with both the mean-wind and turbulent-wind components, driven with meteorological output from a Eulerian gridded model. In this case, STILT was driven by wind fields from the High Resolution Rapid Refresh model (Ikeda et al., 2013), at 3-km grid spacing and hourly frequency, downloaded from NOAA's Air Resources Laboratory.

For each receptor location/time, 1000 air parcels are tracked backward in time for 6 h, during which most parcels have exited the Salt Lake Valley. Previous work has shown that even 200 air parcels can adequately resolve the mobile observations of CO_2 along light rail lines (Fasoli et al., 2018). We increased the air parcel ensemble size five-fold to account for potentially additional variability in species such as NOx and CH_4.

The simulated air parcels mark out the atmospheric "footprint" of the receptor (Lin et al., 2003)—i.e., the source region of air arriving at the receptor. As such, the footprint provides a quantitative link between a potential emission source upwind of the receptor and the concentration change at the receptor, in the absence of chemical transformations. Thus, the footprint serves as a critical piece of information by which unknown sources can be localized, given elevated pollutant concentrations detected by the mobile platform.

Referred to as the Stochastic Lagrangian Monte Carlo (SLMC) source identification method (Fig. 2), we create randomized realizations of emission fields in the potential source region and assess the statistical correlation between the random fields with the observed pollutant variations using the STILT-simulated atmospheric footprints.

The method is based on the expectation that emissions from gridcells within the potential source region which lead to stronger correlations with the observed pollutant concentrations have stronger likelihood to

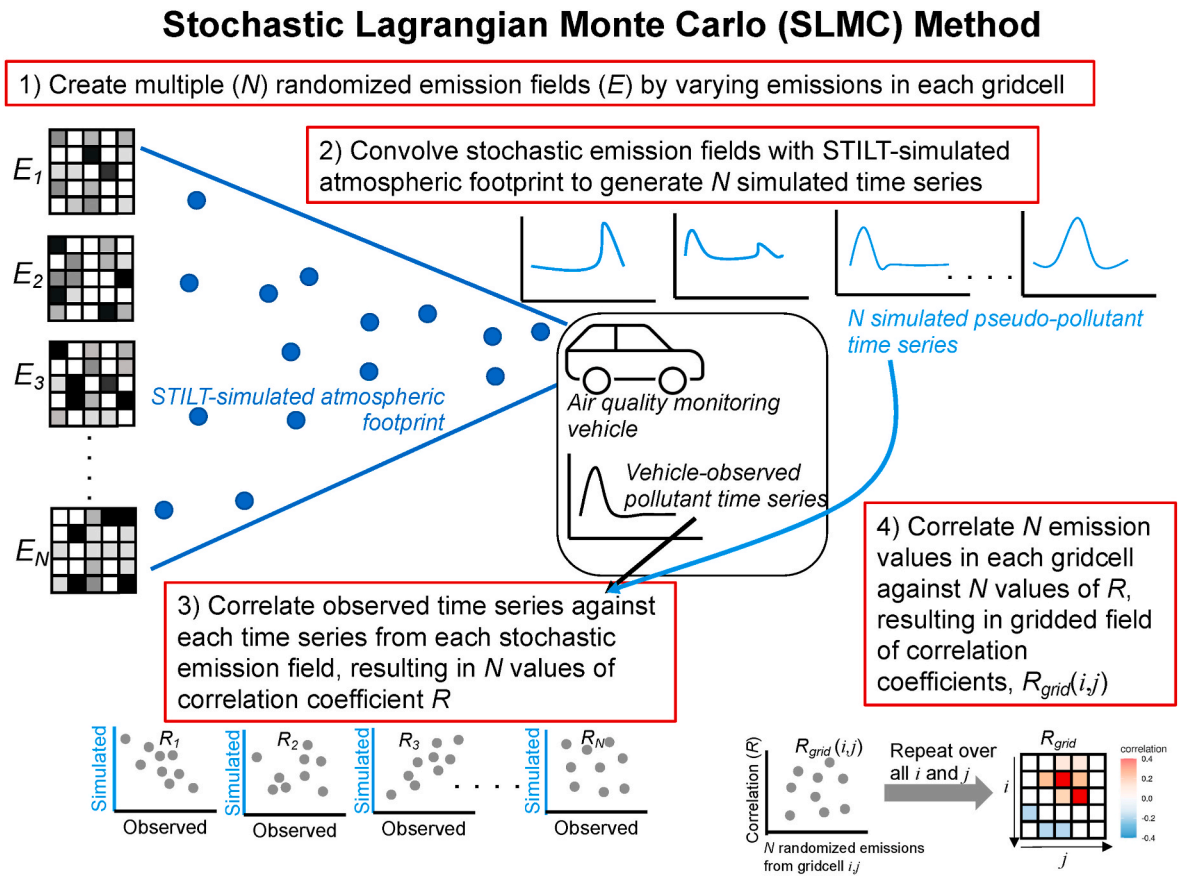

Fig. 2. Schematic summarizing the steps in the Stochastic Lagrangian Monte Carlo method for source localization.

be the actual source of the observed pollution. The SLMC method is illustrated in Fig. 2 and consists of the following steps.

1) Create multiple ($N = 1000$) randomized emission field in potential source region

Each gridcell in the emission field comprising the potential source region (dimensions of which are flexible) is perturbed using a uniform distribution ranging between 0 and 1, representing a normalized emissions flux.

2) Convolve each stochastic realization of emission field with atmospheric footprint to estimate excess concentration at receptors where mobile sampling took place

For each randomized emissions field, calculate a corresponding time series measurement at each receptor location using the atmospheric transport information from the STILT trajectories and the corresponding footprint.

3) Correlate observed time series against time series from each stochastic emission field in 2) to calculate N values of correlation coefficient R

The time series observed by the Google Street View vehicles is compared against each of the simulated time series generated from convolving the randomized field with the footprint. Each comparison yields a correlation coefficient R. Thus N realizations of the randomized emission fields results in N values of R.

4) Correlate the N values of R with each N random emission values for each gridcell in source region

To elucidate the gridcells especially likely to be responsible for the observed concentration fluctuations, we take the N values of R and further correlate the values of R against the N stochastic emission values for each gridcell. This results in a spatial field of correlation coefficients, R_{grid}, one for each gridcell. Gridcells with higher values of R_{grid} are more probable to be a pollution source, thereby helping to localize emission sources.

3. Results

3.1. Spatial patterns of tracer enhancements

The spatial patterns of observed tracer enhancements, based upon all drives throughout the measurement period, are shown in Fig. 3. Each 0.002° × 0.002° gridcell shown is the median of all the observed receptor values. A minimum of 20 repeated visits are necessary to retain the gridcell. The choice of 20 drives derives from a statistical analysis shown in the Supplement (Fig. S6).

The spatial patterns of enhancements in NO_x, $PM_{2.5}$, BC, and CO_2 are dominated by the major highways in the Salt Lake area (Fig. 1). These include a) I-15, bisecting north-south near the center of the domain; b) I-215, the beltway roughly circling the main urban area; and c) I-80, the major west-east highway. The significant enhancements are especially evident for BC_{ex}, which exceeded well >1500 ng m^{-3} along highways.

Traffic-related emissions are well documented in previous studies (Apte et al., 2017; Deshmukh et al., 2020; Targino et al., 2016). Note

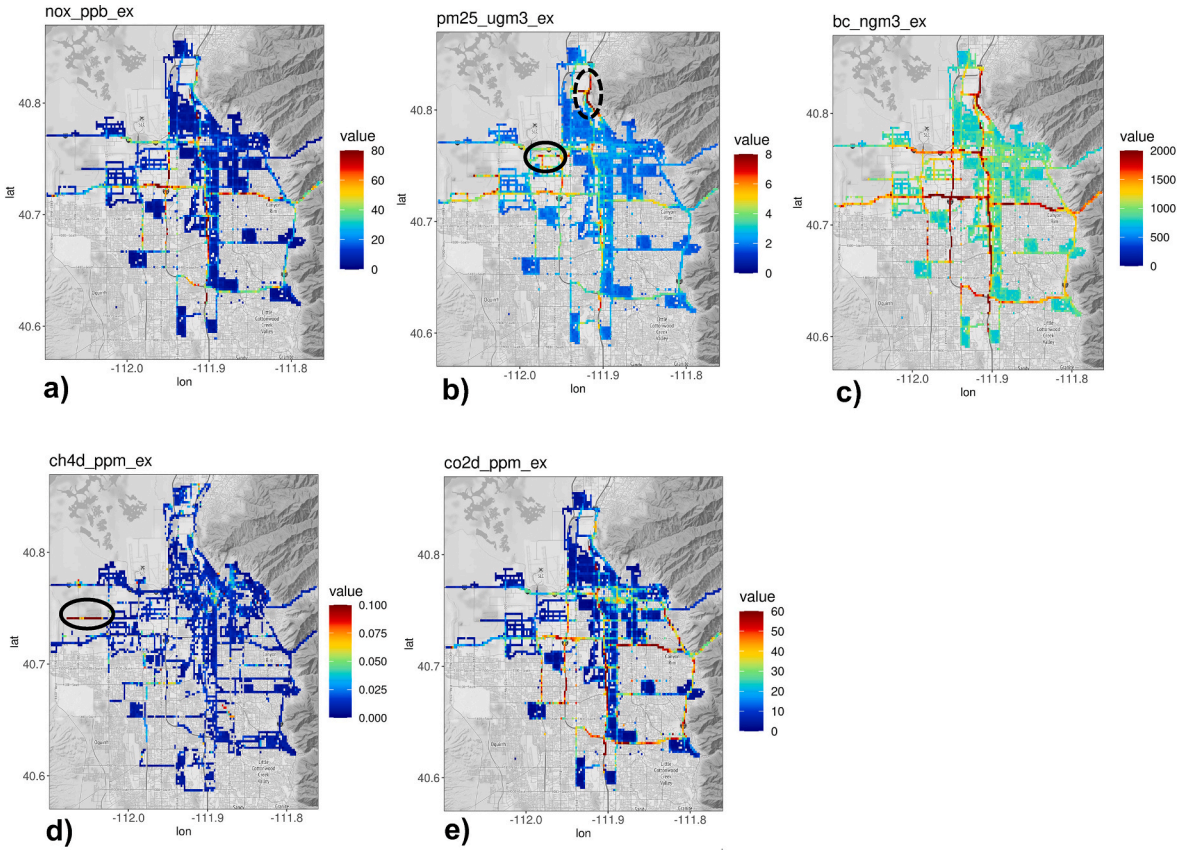

Fig. 3. The spatial patterns of observed pollutant enhancements based upon all drives throughout the measurement period for: a) NOx_{ex} [ppb], b) $PM_{2.5ex}$ [μg m^{-3}], c) BC_{ex} [ng m^{-3}], d) CH_{4ex} [ppm], and e) CO_{2ex} [ppm]. Each 0.002° × 0.002° gridcell shown is the median of all the observed receptor values. A minimum of 20 repeated visits are necessary to retain the gridcell for display. The black ovals indicate specific regions and pollutants used for case studies (Sect. 3.3), with the dashed black oval in b) specifically referring to the gravel pit case (Sect. 3.3.2).

that the polygons that serve as foci of this study (Fig. 1) are, by design, excluding the observations directly on the highways, albeit polygons adjacent to the highways would presumably be affected by the high traffic emissions, as seen in the higher NO_{xex}, $PM_{2.5ex}$, BC_{ex} in the gridcells adjacent to the north-south corridor along I-15. The polygon-aggregated pollutant levels and their relationships to socio-economic variables will be discussed in Sect. 3.2.

The pattern in CH_4 enhancements, observed mainly during summer 2019 when instrumentation was available, is noticeably different from the other species. Instead of the persistent highway signal, CH_4 enhancements are found in "hotspots" that were variable across time and space (Fig. 3d) (Hopkins et al., 2016). The exception is a sustained, elevated CH_4 plume found in the northwestern portion of the sampling domain (black oval in Fig. 3d), just south of the Salt Lake County landfill. This known source of persistent CH_4 emissions from the landfill will be adopted as one of the first case studies to test the Stochastic Lagrangian Monte Carlo (SLMC) source identification method (Sect. 3.3.1). The other case studies will examine the high $PM_{2.5}$ enhancement to the north and just south of the Salt Lake City airport (black ovals in Fig. 3b).

3.2. Polygon-level pollutant enhancements and relationship to socioeconomic variables

Next, we relate the observed pollutant enhancements in each polygon (Sect. 2.4) to several socioeconomic variables from the 2010 U.S. Census. The spatial patterns between enhancements in BC, $PM_{2.5}$, and NO_x are qualitatively similar (Fig. 4). These pollutants exhibit elevated values in polygons clustered in a north-south axis, along the I-15 freeway corridor (Fig. 1). Elevated values are also found in the industrial area in the northwestern portion of the domain, just south and southwest of the Salt Lake International Airport. Individual correlations between pollutant levels and socioeconomic variables in the different polygons are shown in Fig. 5. Strong correlations ($R > 0.8$) are found between $PM_{2.5ex}$, NOx_{ex}, and BC_{ex}, suggesting co-emitted or co-located pollutant sources and reflecting the similar spatial patterns seen in Fig. 4, similar to results from a previous study (Brantley et al., 2014a). The pollutant levels are negatively correlated with population density and income (with $PM_{2.5}$ being statistically insignificant) while positively correlated with the percent of Black residents.

These pollutant-socioeconomic relationships were confirmed with multiple linear regression, using the socioeconomic variables to predict pollutant levels (Table S2). The multiple linear regression also underscored the fact that areas with elevated pollutant levels were associated with lower income, lower population density, and higher percent of Black residents. Population density here can be thought of as a proxy for residential neighborhoods: density is higher for purely residential polygons while lower for polygons with a significant degree of industrial activity.

The polygons with higher percent of Black residents are concentrated in the north-south axis along the I-15 freeway (Fig. S5)—indeed, where pollutant levels are elevated (Fig. 4). It is worth noting that the I-15 corridor corresponds to neighborhoods that have been "red-lined"—i.e., labelled as "hazardous" or "definitely declining" as part of discriminatory practices carried out by the federally-supported Home Owners' Loan Corporation in the 1930s and 1940s (Nelson et al., 2022).

In summary, detailed mobile sampling in Salt Lake City has reaffirmed what has also been reported in other cities: minorities and lower income groups are exposed to more pollutants (Chambliss et al., 2021; Demetillo et al., 2021; Lane et al., 2022), and that regions with high pollutant levels can trace their legacy to redlining practices decades ago

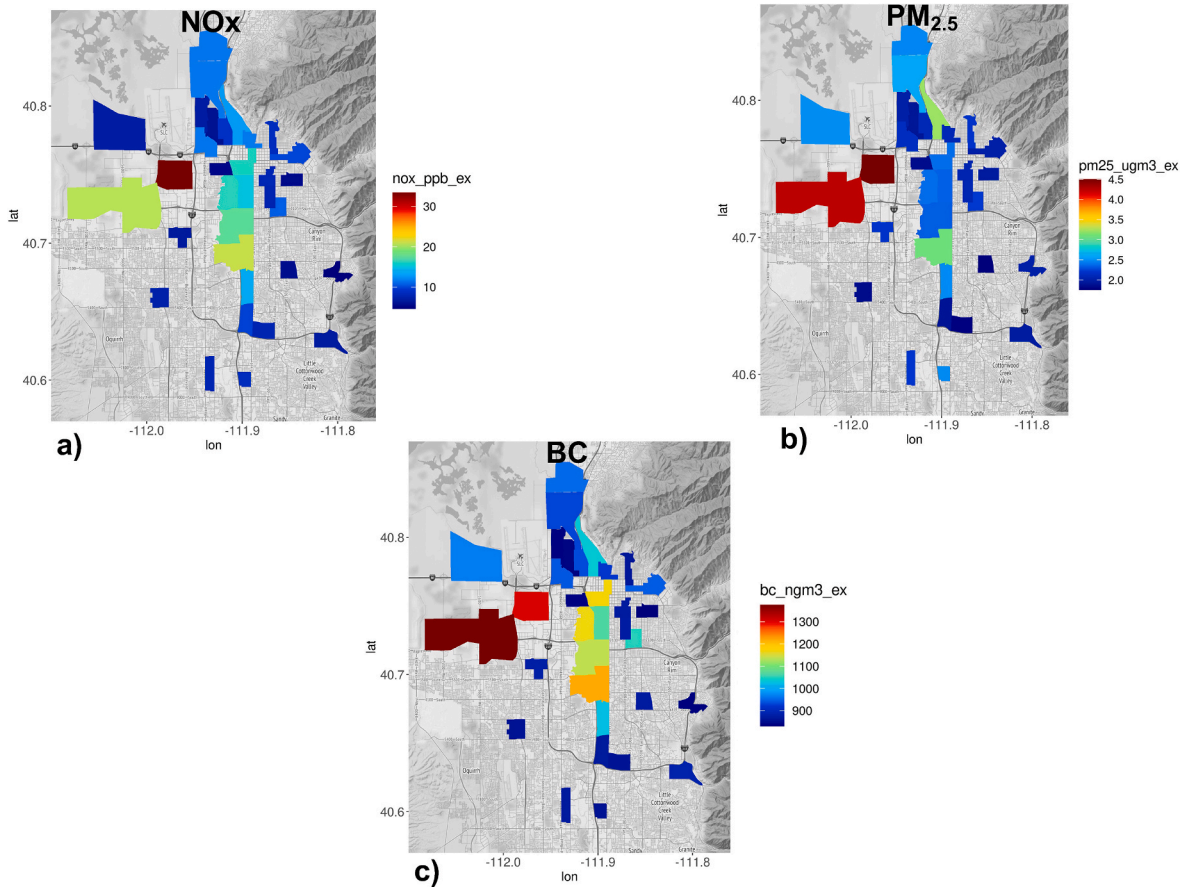

Fig. 4. The polygon-level medians of daily averages from all sampling days for a) NOx_{ex} [ppb], b) $PM_{2.5ex}$ [μg m^{-3}], and c) BC_{ex} [ng m^{-3}]. The vehicle was required to spend a minimum of 1 h in a polygon on a particular day for the data to be included for polygon-level analyses.

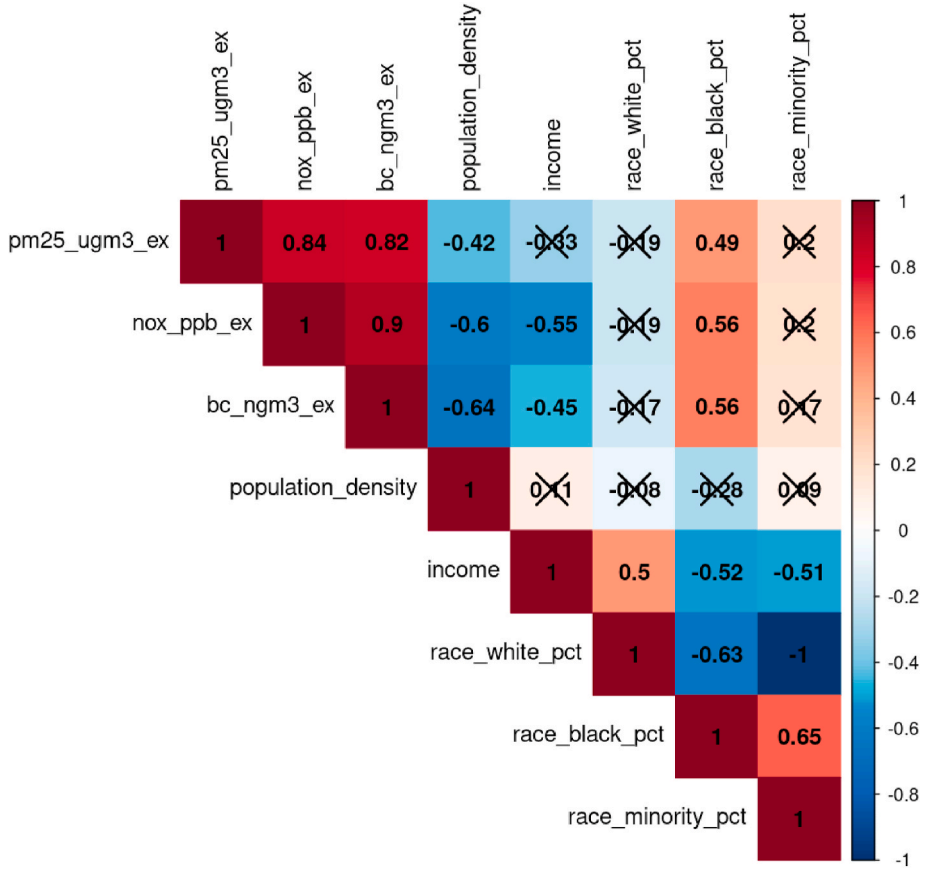

Fig. 5. Correlation strengths (*R*) between polygon-level median enhancements in pollutants (NOx, $PM_{2.5}$, BC) and socioeconomic variables (population density, income, % white residents, % black residents, and % minority residents). Statistically less significant correlations with p-value >0.05 are crossed out with an "X".

(Lane et al., 2022).

3.3. Case studies

Here we present case studies in which the Stochastic Lagrangian Monte Carlo (SLMC) source identification method was adopted to identify the potential location(s) of sources, after accounting for atmospheric transport through the STILT model. We illustrate the results through case studies. The first two are for known sources—a landfill source for a gaseous species (methane) and a gravel pit for particulates ($PM_{2.5}$). After examining the behavior of the SLMC method for the known sources, the method is applied to an instance when sources in an industrial region are not known a priori.

3.3.1. Case study 1: Landfill

Elevated CH_4 was observed commonly to the northwest portion of the study domain (black oval in Fig. 3d), where a landfill is located. Landfills are well-recognized as a significant source of methane (Cusworth et al., 2020), as the third largest anthropogenic source accounting for ~17% of all anthropogenic methane emissions in the U.S. (US Environmental Protection Agency, 2022).

All of the receptor-level methane observations (CH_{4ex}), along with their aggregated footprints simulated by STILT, are shown in Fig. 6a. These footprints, along with the receptor-level observations, were used within SLMC to determine the gridcells most responsible for the observed plumes within an user-determined "search region", chosen here using the satellite image of the landfill boundaries. The output of the algorithm is a set of correlation values, one for each gridcell within the search region (Fig. 2). Gridcells with higher correlations indicate stronger statistical relationships between emissions from their locations to the observed plumes at the receptors. These correlation values are shown in Fig. 6b for a rectangular search region with an area of 14.9 km^2. The gridcells with the highest correlations are found within the landfill (Google Earth image shown in Fig. 6d), precisely where high CH_4 emissions are expected.

As a sensitivity test, the search region is enlarged greatly to span the range of the observation receptors, to cover a much larger area of 44.8 km^2 (Fig. 6c). In this case, the clear hotspot over the landfill is no longer evident. Instead, SLMC yields a large number of gridcells with weakly positive correlation values, with no clear focal points. This example highlights the importance of constraining, a priori, the size of a search region. Otherwise, the large number of degrees of freedom represented by the numerous gridcells would preclude the emission source to be adequately located.

We also carried out a sensitivity test varying the number of drives incorporated into the SLMC calculation. The total number of 27 drives for the landfill case study was randomly sub-sampled (without replacement) for input into SLMC, and the randomized sampling was repeated 10 times. The correlation map averaged over the 10 realizations for different drive numbers is then shown in Fig. S7. The correlation strengths are diffuse for 1, 2, and 4 drives, with the landfill starting to emerge in the gridcells with stronger correlations >10 drives. By 20 drives, the landfill emerged as the focal area, with clearly elevated correlations. It is worth noting that the exact number of drives needed to localize the source would depend case-by-case on the wind patterns and drives in relationship to the source locations—e.g., whether the drive happened to include sampling on the road just south of the landfill (Fig. 6b). Regardless, we speculate that at least ~10 drives are needed for source localization; a similar number emerged for the gravel pit case study discussed below (Fig. S8). It is also probable that increasing the number of drives would enable source localization with a larger search region; however, we were not able to evaluate that hypothesis in this

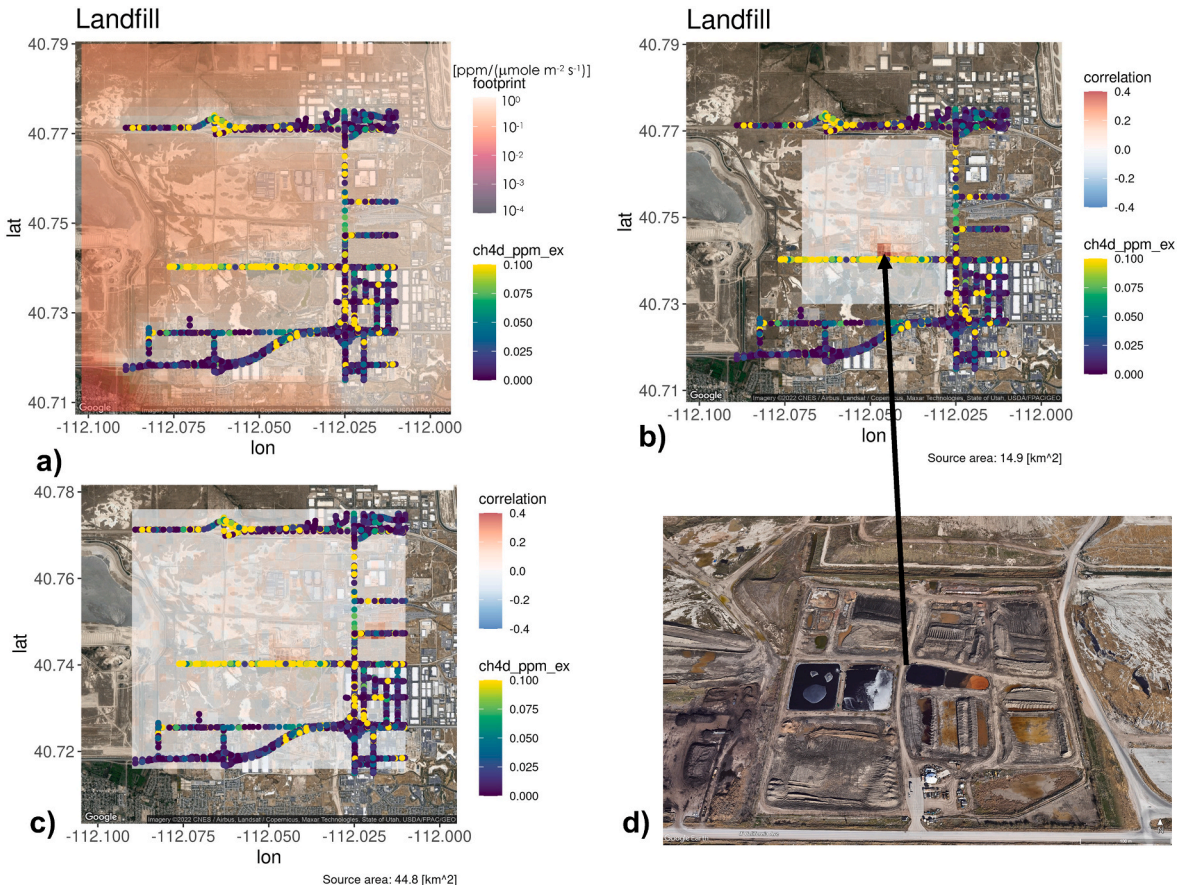

Fig. 6. Case study involving the use of the SLMC source identification method to determine evaluate the CH_4 emission hotspot near a landfill (black oval in Fig. 3d). a) The aggregate STILT-simulated footprint derived from summing the footprints of all receptors associated with the vehicle-based sampling. The observed CH_{4ex} [ppm] at each receptor is shown in a separate colorscale as well. b) Result of the SLMC technique indicating the correlation (R) between emissions from specific gridcells and the observed CH_{4ex} over a search region of 14.9 km^2. c) Sensitivity of SLMC to the search region, covering an area of 44.8 km^2, much larger than in b). d) Google Earth image of the landfill—precisely the gridcells with the highest correlations in b).

study because we only had 27 total drives adjacent to the landfill.

3.3.2. *Case study 2: Gravel pit*

The other case study for which we tested the SLMC was the northern portion of the study domain (dashed black oval in Fig. 3b), in which elevated $PM_{2.5}$ levels are observed, and where a prominent gravel pit is located (Fig. 7a). Gravel pits are well known as sources of $PM_{2.5}$ and particulates in general (Peng et al., 2016; Mendez-Astudillo et al., 2022). SLMC successfully identifies a broad region of the gravel pit with higher correlations, with especially higher values over gridcells where the gravel operation is close to the road (Fig. 7c). Similar to the landfill example, these gridcells with higher correlations emerge as the number of drives are increased, especially coming into focus with 20 drives (Fig. S8).

The result of the landfill and gravel pit examples is a more spatially refined estimate for the location of actual emissions at each facility: from the full area, to a more precise 200 m grid box. An example of the utility of this method would be to determine a specific location of a leak, identified by mobile monitoring, on an oil and gas field where numerous potential source locations for a methane leak would exist. More importantly, this method can be used to identify unknown source locations, as demonstrated in the next example.

3.3.3. *Case study 3: Unknown $PM_{2.5}$ hotspot*

In the last case study, the SLMC was applied to an instance where source(s) were unknown a priori. The region of investigation here is an industrial area just south of the Salt Lake City airport (black oval in Fig. 3b) where plumes of $PM_{2.5}$ were observed (Fig. 8a). SLMC yielded the highest correlations in a number of gridcells, one of which containing mounds of gravel can be seen in Google Earth imagery, belonging to a construction materials company (Fig. 8d) whose location is indicated by the black arrow. Such an operation is understandably a source for particulates and elevated $PM_{2.5}$.

However, additional high correlations are seen in the two gridcells to the south of the gravel mound, as well as to the west, across the road. To minimize the possibility that erroneous source location can stem from errors in the HRRR windfield driving STILT, we further filtered out drives when the HRRR windfield exhibited biases when compared against nearby surface weather stations in the MesoWest network (Horel et al., 2002). Specifically, if the U- (eastward) or V- (northward) components of the wind vector from HRRR pointed in the wrong direction during the time when the vehicle was in the industrial area shown in Fig. 8, that drive was removed from consideration. Under this criterion, 17 drives were removed out of the 55 drives that passed through the industrial area.

The result from SLMC after removing times/drives with erroneous windfields is shown in Fig. 8c. The high correlations in the two gridcells south of the gravel mound—with no obvious sources—no longer exists, while a gridcell with high correlation just west of the gravel mound, across the N–S running road, remains. This is the locale of a freight/trucking operation; as such, the heavy-duty trucks can account for the source of $PM_{2.5}$ (Bureau of Transportation Statistics, 2021).

Thus, we see that SLMC has successfully located sources of $PM_{2.5}$ that were not known a priori. However, we also see that SLMC is sensitive to

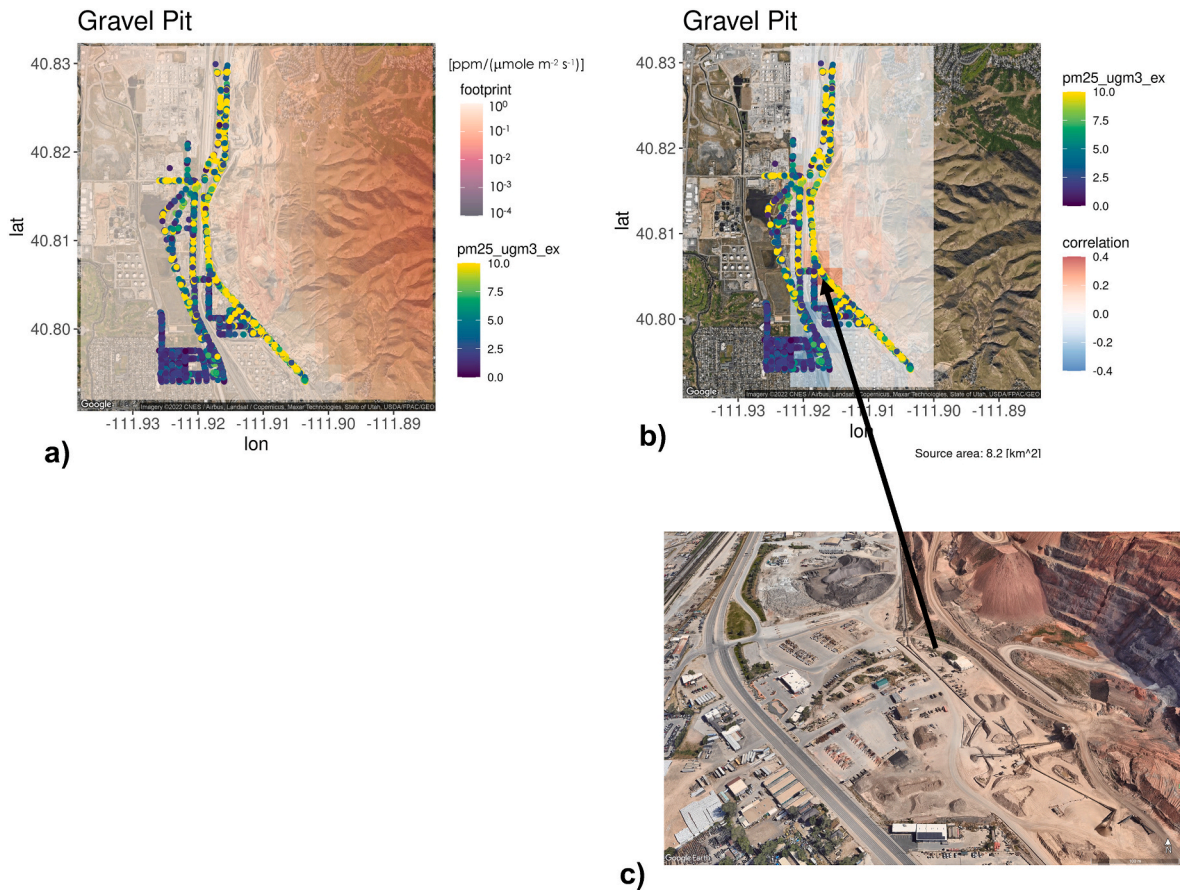

Fig. 7. Similar to Fig. 6, but for a case study involving the use of the SLMC source identification method to determine the $PM_{2.5}$ emission hotspot near a gravel pit operation (dashed black oval in Fig. 3b). The Google Earth image in c) shows the gravel pit—corresponding to the gridcells with the highest correlations in b).

the driving meteorology: erroneous winds can lead to inaccurate source localization, as seen in Fig. 8b. Additional considerations by comparing the driving windfields against observations can help alleviate such potential errors.

4. Discussion

The original scientific questions are reproduced here in italics, along with results from this study:

- *How are pollutants distributed across Salt Lake City, and how do pollution patterns in residential neighborhoods relate to socioeconomic patterns?*

Distributions in pollutant enhancements (Fig. 3) follow general patterns expected from traffic and industrial activities. Pollutants are higher in neighborhoods with lower income and higher percentage of Black residents (Figs. 4 and 5), broadly in accordance with the emerging environment justice literature (Chambliss et al., 2021; Demetillo et al., 2021; Lane et al., 2022).

- *By utilizing detailed atmospheric modeling, can on-road hotspots detect and localize non-road emission sources?*

The new Stochastic Lagrangian Monte Carlo (SLMC) method appears to be able to identify and localize sources away from the road, based on the mobile observations. This was confirmed by two well-known sources serving as test cases: a large landfill methane source (Fig. 6) and a gravel pit $PM_{2.5}$ source (Fig. 7). When applied to an industrial area, SLMC localized a construction materials company and a freight/trucking operation—both plausible $PM_{2.5}$ sources (Fig. 8).

The success of the SLMC method depends on multiple factors. First, the simulated atmospheric transport needs to accurately link observed concentrations to upwind potential sources, so times with erroneous winds need to be accounted for, such as through removal of erroneous times (Fig. 8c) or through bias correction using observed winds. Second, the potential source region in which to search for emission sources cannot be too large (Fig. 6c), lest the degrees of freedom expand to a degree that prevents successful localization. Third, the number of drives sampling the pollution source needs to be adequate, (including sufficient days where sampling occurs downwind of the source), or a well-defined source may not emerge (Figs. S7 and S8). While the exact sampling requirements may depend on the details of each case—e.g., distance of source relative to the road, source strength, wind patterns, and driving patterns—it appears that at least 10 drives are needed in the land fill and gravel pit test cases to successfully localize the source (Figs. S7 and S8). For intermittent sources, the sampling requirements would be even more stringent, in order for the mobile sampling to capture enough cases with concentration enhancements.

Monte Carlo methods more sophisticated than the SLMC method can potentially be adopted in the future, including meteorological ensembles and detailed emission characteristics (Lucas et al., 2017), at the cost of increased computational expense and coding complexity.

With the availability of source localization techniques like the SLMC or related methods, the potential for mobile air quality observational platforms serving as "roving sentinels" can be realized. Once a pollution source is identified through source localization, the sampling pattern of the vehicle could be modified to target more drives dedicated to the identified source—e.g., circling the source or even parking the vehicle downwind of the source. In turn, regulatory measures to mitigate the-

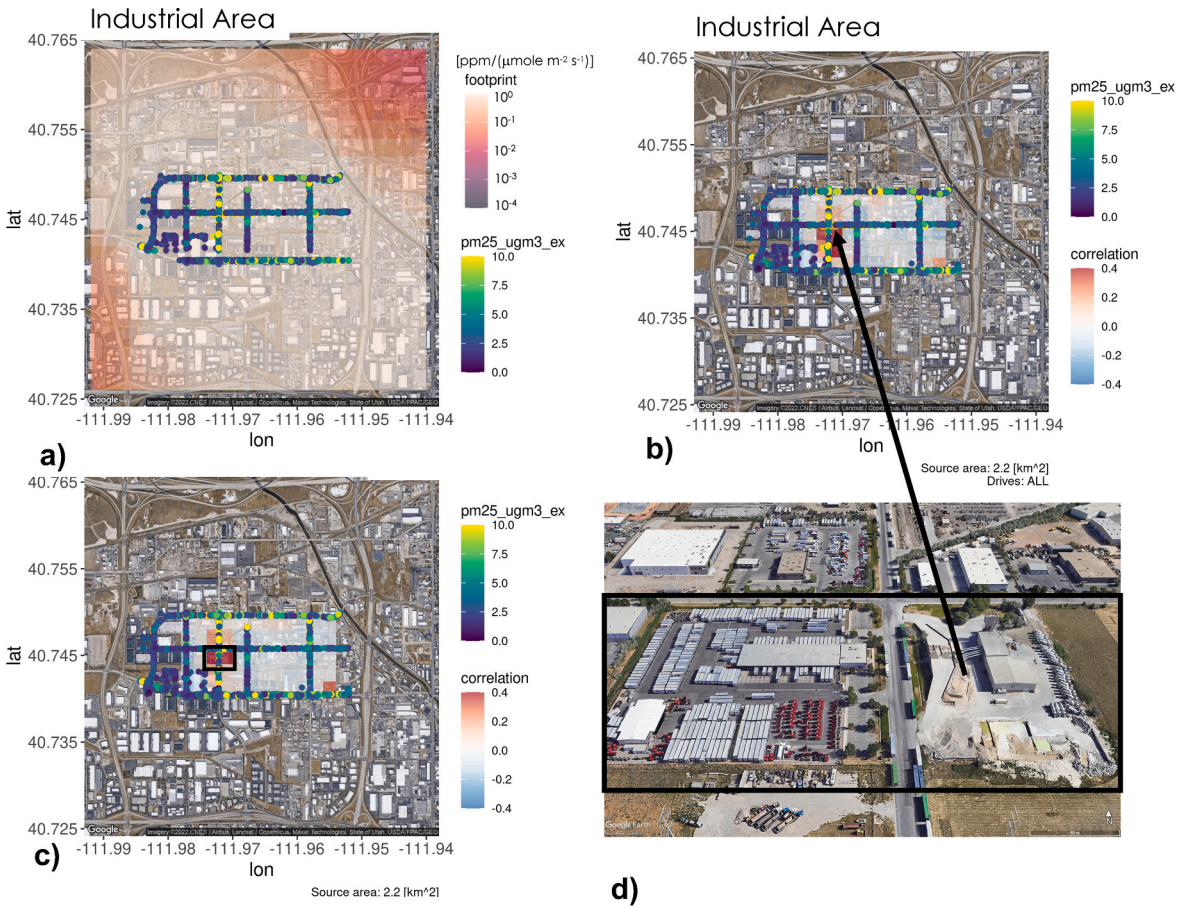

Fig. 8. Similar to Figs. 6 and 7, but for a case study involving the use of the SLMC source identification method to determine the $PM_{2.5}$ emission hotspot in an industrial area just south of the SLC airport with unknown sources (black oval in Fig. 3b). Results of the SLMC technique are shown b) for all 55 drives and c) after removing 17 drives in which the U- or V-components of the wind vector were pointing in the wrong direction, as informed from a comparison against surface weather stations. The Google Earth image in d) show the construction materials company to the right and freight/trucking company to the left corresponding to the gridcells with the highest correlations in c), marked with the black box.

identified pollution sources can also be considered.

Author Contribution

John C. Lin: Conceptualization, Supervision, Project administration, Writing – original draft. Ben Fasoli: Conceptualization, Methodology, Software, Data curation, Formal analysis. Logan Mitchell: Conceptualization, Methodology, Investigation, Formal analysis. Ryan Bares: Methodology, Investigation. Francesca Hopkins: Investigation, Resources. Tammy M. Thompson: Conceptualization, Project administration, Writing – review & editing. Ramón A. Alvarez: Conceptualization, Supervision, Project administration, Funding acquisition.

Declaration of competing interest

The authors declare that they have no known competing financial interests or personal relationships that could have appeared to influence the work reported in this paper.

Data availability

The Google Street View-based air quality observations can be downloaded at: https://doi.org/10.5281/zenodo.7605718.

Acknowledgements

We acknowledge funding from Environmental Defense Fund, whose work is supported by gifts from Signe Ostby, Scott Cook, and Valhalla Foundation. We thank Karin Tuxen-Bettman from Google, the multiple drivers of the two Google Street View vehicles for their dedication, and netMercury for lending us a Los Gatos Research Micro-portable greenhouse gas analyzer. We appreciate the organizational skills of Megan Dupuy-Todd. JCL would like to thank Alex Jacques, John Horel, and James Mineau for helpful discussions. The support and resources from the Center for High Performance Computing at the University of Utah and Google Earth for data visualizations are gratefully acknowledged. The Google Street View-based air quality observations can be downloaded at: https://doi.org/10.5281/zenodo.7605718.

Appendix A. Supplementary data

Supplementary data to this article can be found online at https://doi.org/10.1016/j.atmosenv.2023.119995.

References

Alexeeff, S.E., Roy, A., Shan, J., Liu, X., Messier, K., Apte, J.S., Portier, C., Sidney, S., Van Den Eeden, S.K., 2018. High-resolution mapping of traffic related air pollution with Google street view cars and incidence of cardiovascular events within neighborhoods in Oakland, CA. Environ. Health 17, 38. https://doi.org/10.1186/s12940-018-0382-1.

Apte, J.S., Messier, K.P., Gani, S., Brauer, M., Kirchstetter, T.W., Lunden, M.M., Marshall, J.D., Portier, C.J., Vermeulen, R.C.H., Hamburg, S.P., 2017. High-resolution air pollution mapping with google street view cars: exploiting big data. Environ. Sci. Technol. 51, 6999–7008. https://doi.org/10.1021/acs.est.7b00891.

Bares, R., Lin, J.C., Hoch, S.W., Baasandorj, M., Mendoza, D.L., Fasoli, B., Mitchell, L., Catharine, D., Stephens, B.B., 2018. The wintertime covariation of CO2 and criteria pollutants in an urban valley of the Western United States. J. Geophys. Res: Atmos. 123, 2684–2703. https://doi.org/10.1002/2017JD027917.

Brantley, H.L., Hagler, G.S.W., Herndon, S.C., Massoli, P., Bergin, M.H., Russell, A.G., 2019. Characterization of spatial air pollution patterns near a large railyard area in Atlanta, Georgia. Int. J. Environ. Res. Public Heal. 16 https://doi.org/10.3390/ijerph16040535.

Brantley, H.L., Hagler, G.S.W., Kimbrough, E.S., Williams, R.W., Mukerjee, S., Neas, L. M., 2014a. Mobile air monitoring data-processing strategies and effects on spatial air pollution trends. Atmos. Meas. Tech. 7, 2169–2183. https://amt.copernicus.org/articles/7/2169/2014/.

Brantley, H.L., Thoma, E.D., Squier, W.C., Guven, B.B., Lyon, D., 2014b. Assessment of methane emissions from oil and gas production pads using mobile measurements. Environ. Sci. Technol. 48, 14508–14515. https://doi.org/10.1021/es503070q.

Bureau of Transportation Statistics, 2021. *National Transportation Statistics*. Washington, D.C., Estimated U.S. Average Vehicle Emissions Rates Per Vehicle by Vehicle Type Using Gasoline and Diesel. (Accessed 24 November 2022).

Caubel, J.J., Cados, T.E., V Preble, C., Kirchstetter, T.W., 2019. A distributed network of 100 black carbon sensors for 100 Days of air quality monitoring in west oakland, California. Environ. Sci. Technol. 53, 7564–7573. https://doi.org/10.1021/acs.est.9b00282.

Chambliss, S.E., Pinon, C.P.R., Messier, K.P., LaFranchi, B., Upperman, C.R., Lunden, M. M., Robinson, A.L., Marshall, J.D., Apte, J.S., 2021. Local- and regional-scale racial and ethnic disparities in air pollution determined by long-term mobile monitoring. Proc. Natl. Acad. Sci. U.S.A. 118, e2109249118 https://doi.org/10.1073/pnas.2109249118.

Cohen, A.J., Brauer, M., Burnett, R., Anderson, H.R., Frostad, J., Estep, K., Balakrishnan, K., Brunekreef, B., Dandona, L., Dandona, R., Feigin, V., Freedman, G., Hubbell, B., Jobling, A., Kan, H., Knibbs, L., Liu, Y., Martin, R., Morawska, L., Pope III, C.A., Shin, H., Straif, K., Shaddick, G., Thomas, M., van Dingenen, R., van Donkelaar, A., Vos, T., Murray, C.J.L., Forouzanfar, M.H., 2017. Estimates and 25-year trends of the global burden of disease attributable to ambient air pollution: an analysis of data from the Global Burden of Diseases Study 2015. The Lancet 389, 1907–1918. https://doi.org/10.1016/S0140-6736(17)30505-6.

Cusworth, D.H., Duren, R.M., Thorpe, A.K., Tseng, E., Thompson, D., Guha, A., Newman, S., Foster, K.T., Miller, C.E., 2020. Using remote sensing to detect, validate, and quantify methane emissions from California solid waste operations. Environ. Res. Letts. 15, 54012. https://doi.org/10.1088/1748-9326/ab7b99.

Delaria, E.R., Kim, J., Fitzmaurice, H.L., Newman, C., Wooldridge, P.J., Worthington, K., Cohen, R.C., 2021. The Berkeley Environmental Air-quality and CO2 Network: field calibrations of sensor temperature dependence and assessment of network scale CO2 accuracy. Atmos. Meas. Tech. Discuss. 1–30, 2021. https://amt.copernicus.org/preprints/amt-2021-120/.

Demetillo, M.A.G., Harkins, C., McDonald, B.C., Chodrow, P.S., Sun, K., Pusede, S.E., 2021. Space-based observational constraints on NO2 air pollution inequality from diesel traffic in major US cities. Geophys. Res. Lett. 48, e2021GL094333 https://doi.org/10.1029/2021GL094333, 10.1029/2021GL094333.

Deshmukh, P., Kimbrough, S., Krabbe, S., Logan, R., Isakov, V., Baldauf, R., 2020. Identifying air pollution source impacts in urban communities using mobile monitoring. Sci. Total Environ. 715, 136979 https://doi.org/10.1016/j.scitotenv.2020.136979. https://www.sciencedirect.com/science/article/pii/S0048969720304897.

Dockery, D.W., Pope, C.A., Xu, X., Spengler, J.D., Ware, J.H., Fay, M.E., Ferris, B.G., Speizer, F.E., 1993. An association between air pollution and mortality in six U.S. Cities. N. Engl. J. Med. 329, 1753–1759.

Fasoli, B., Lin, J.C., Bowling, D.R., Mitchell, L., Mendoza, D., 2018. Simulating atmospheric tracer concentrations for spatially distributed receptors: updates to the Stochastic Time-Inverted Lagrangian Transport model's R interface (STILT-R version 2). Geosci. Model Dev. (GMD) 11, 2813–2824. https://www.geosci-model-dev.net/11/2813/2018/.

Feenstra, B., Papapostolou, V., Hasheminassab, S., Zhang, H., Der Boghossian, B., Cocker, D., Polidori, A., 2019. Performance evaluation of twelve low-cost PM2.5 sensors at an ambient air monitoring site. Atmos. Environ. 216, 116946 https://doi.org/10.1016/j.atmosenv.2019.116946. https://www.sciencedirect.com/science/article/pii/S1352231019305850.

Fruin, S., Urman, R., Lurmann, F., McConnell, R., Gauderman, J., Rappaport, E., Franklin, M., Gilliland, F.D., Shafer, M., Gorski, P., Avol, E., 2014. Spatial variation in particulate matter components over a large urban area. Atmos. Environ. 83, 211–219. https://doi.org/10.1016/j.atmosenv.2013.10.063.

Gu, P., Li, H.Z., Ye, Q., Robinson, E.S., Apte, J.S., Robinson, A.L., Presto, A.A., 2018. Intracity variability of particulate matter exposure is driven by carbonaceous sources and correlated with land-use variables. Environ. Sci. Technol. 52, 11545–11554. https://doi.org/10.1021/acs.est.8b03833.

Hoek, G., Krishnan, R.M., Beelen, R., Peters, A., Ostro, B., Brunekreef, B., Kaufman, J.D., 2013. Long-term air pollution exposure and cardio- respiratory mortality: a review. Environ. Health (Lond.) 12, 43. https://doi.org/10.1186/1476-069X-12-43.

Hopkins, F.M., Ehleringer, J.R., Bush, S.E., Duren, R.M., Miller, C.E., Lai, C.-T., Hsu, Y.-K., Carranza, V., Randerson, J.T., 2016. Mitigation of methane emissions in cities: how new measurements and partnerships can contribute to emissions reduction strategies. Earths Future 4, 408–425. https://doi.org/10.1002/2016EF000381.

Horel, J., Splitt, M., Dunn, L., Pechmann, J., White, B., Ciliberti, C., Lazarus, S., Slemmer, J., Zaff, D., Burks, J., 2002. Mesowest: cooperative mesonets in the western United States. Bull. Am. Meteorol. Soc. 83, 211–225. doi:10.1175/1520-0477(2002)083%3C0211:MCMITW%3E2.3.CO;2.

Hu, Y., Dai, G., Fan, J., Wu, Y., Zhang, H., 2016. BlueAer: a fine-grained urban PM2.5 3D monitoring system using mobile sensing. IEEE INFOCOM 2016 - The 35th Annual IEEE International Conference on Computer Communications 1–9.

Ikeda, K., Steiner, M., Pinto, J., Alexander, C., 2013. Evaluation of Cold-Season Precipitation Forecasts Generated by the Hourly Updating High-Resolution Rapid Refresh Model, vol. 28. Weather Forecast, pp. 921–939.

Jackson, R.B., Down, A., Phillips, N.G., Ackley, R.C., Cook, C.W., Plata, D., Zhao, K., 2014. Natural gas pipeline leaks across Washington, DC. Environ. Sci. Technol. 48, 2051–2058.

Kaur, S., Nieuwenhuijsen, M.J., Colvile, R.N., 2007. Fine particulate matter and carbon monoxide exposure concentrations in urban street transport microenvironments. Atmos. Environ. 41, 4781–4810. https://doi.org/10.1016/j.atmosenv.2007.02.002. https://www.sciencedirect.com/science/article/pii/S1352231007001343.

Lane, H.M., Morello-Frosch, R., Marshall, J.D., Apte, J.S., 2022. Historical redlining is associated with present-day air pollution disparities in U.S. Cities. Environ. Sci. Technol. Lett. 9, 345–350. https://doi.org/10.1021/acs.estlett.1c01012.

Lin, J.C., Gerbig, C., Wofsy, S.C., Andrews, A.E., Daube, B.C., Davis, K.J., Alibert, C.A., 2003. A near-field tool for simulating the upstream influence of atmospheric observations: the Stochastic Time-Inverted Lagrangian Transport (STILT) model. J. Geophys. Res. 108, 4493. https://doi.org/10.1029/2002JD003161.

Loughner, C., Fasoli, B., Stein, A.F., Lin, J.C., 2021. Incorporating features from the Stochastic Time-Inverted Lagrangian Transport (STILT) model into the Hybrid Single-Particle Lagrangian Integrated Trajectory (HYSPLIT) model: a unified dispersion model for time-forward and time-reversed applications. J. Appl. Meteorol. Climatol. 60, 799–810. https://doi.org/10.1175/JAMC-D-20-0158.1.

Lucas, D.D., Simpson, M., Cameron-Smith, P., Baskett, R.L., 2017. Bayesian inverse modeling of the atmospheric transport and emissions of ācontrolled tracer release from ānuclear power plant. Atmos. Chem. Phys. 17, 13521–13543. https://acp.copernicus.org/articles/17/13521/2017/.

Mendez-Astudillo, J., Caetano, E., Pereyra-Castro, K., 2022. Synergy between the urban heat island and the urban pollution island in Mexico city during the dry season. Aerosol Air Qual. Res. 22, 210278 https://doi.org/10.4209/aaqr.210278.

Miller, D.J., Actkinson, B., Padilla, L., Griffin, R.J., Moore, K., Lewis, P.G.T., Gardner-Frolick, R., Craft, E., Portier, C.J., Hamburg, S.P., Alvarez, R.A., 2020. Characterizing elevated urban air pollutant spatial patterns with mobile monitoring in Houston, Texas. Environ Sci Technol. https://doi.org/10.1021/acs.est.9b05523.

Mitchell, L.E., Crosman, E.T., Jacques, A.A., Fasoli, B., Leclair-Marzolf, L., Horel, J., Bowling, D.R., Ehleringer, J.R., Lin, J.C., 2018. Monitoring of greenhouse gases and pollutants across an urban area using a light-rail public transit platform. Atmos. Environ. 187, 9–23. https://doi.org/10.1016/j.atmosenv.2018.05.044.

Morawska, L., Thai, P.K., Liu, X., Asumadu-Sakyi, A., Ayoko, G., Bartonova, A., Bedini, A., Chai, F., Christensen, B., Dunbabin, M., Gao, J., Hagler, G.S.W., Jayaratne, R., Kumar, P., Lau, A.K.H., Louie, P.K.K., Mazaheri, M., Ning, Z., Motta, N., Mullins, B., Rahman, M.M., Ristovski, Z., Shafiei, M., Tjondronegoro, D., Westerdahl, D., Williams, R., 2018. Applications of low-cost sensing technologies for air quality monitoring and exposure assessment: how far have they gone? Environ. Int. 116, 286–299. https://doi.org/10.1016/j.envint.2018.04.018.

Nelson, R.K., Winling, L., Marciano, R., Connolly, N., Al, E., 2022. Mapping Inequality. American Panorama. https://dsl.richmond.edu/panorama/redlining/. (Accessed 23 November 2022).

Padilla, L.E., Ma, G.Q., Peters, D., Dupuy-Todd, M., Forsyth, E., Stidworthy, A., Mills, J., Bell, S., Hayward, I., Coppin, G., Moore, K., Fonseca, E., Popoola, O.A.M., Douglas, F., Slater, G., Tuxen-Bettman, K., Carruthers, D., Martin, N.A., Jones, R.L., Alvarez, R.A., 2021. New methods to derive street-scale spatial patterns of air pollution from mobile monitoring. Atmos. Environ. 118851 https://doi.org/10.1016/j.atmosenv.2021.118851.

Pekney, N.J., Davidson, C.I., Zhou, L., Hopke, P.K., 2006. Application of PSCF and CPF to PMF-modeled sources of PM2.5 in pittsburgh. Aerosol Sci. Technol. 40, 952–961.

Peng, X., Shi, G.-L., Zheng, J., Liu, J.-Y., Shi, X.-R., Xu, J., Feng, Y.-C., 2016. Influence of quarry mining dust on PM2.5 in a city adjacent to a limestone quarry: seasonal characteristics and source contributions. Sci. Total Environ. 550, 940–949. https://doi.org/10.1016/j.scitotenv.2016.01.195. https://www.sciencedirect.com/science/article/pii/S0048969716301917.

Pope, C.A., 2000. Epidemiology of fine particulate air pollution and human health: biologic mechanisms and who's at risk? Environ. Health Perspect. 108, 713–723.

Robinson, E.S., Gu, P., Ye, Q., Li, H.Z., Shah, R.U., Apte, J.S., Robinson, A.L., Presto, A.A., 2018. Restaurant impacts on outdoor air quality: elevated organic aerosol mass from restaurant cooking with neighborhood-scale plume extents. Environ. Sci. Technol. 52, 9285–9294. https://doi.org/10.1021/acs.est.8b02654.

Seto, K.C., Güneralp, B., Hutyra, L.R., 2012. Global forecasts of urban expansion to 2030 and direct impacts on biodiversity and carbon pools. Proc. Natl. Acad. Sci. U. S. A 109, 16083–16088. http://www.ncbi.nlm.nih.gov/pubmed/22988086. (Accessed 12 June 2017).

Shah, R.U., Robinson, E.S., Gu, P., Robinson, A.L., Apte, J.S., Presto, A.A., 2018. High-spatial-resolution mapping and source apportionment of aerosol composition in Oakland, California, using mobile aerosol mass spectrometry. Atmos. Chem. Phys. 18, 16325–16344. https://acp.copernicus.org/articles/18/16325/2018/.

Targino, A.C., Gibson, M.D., Krecl, P., Rodrigues, M.V.C., dos Santos, M.M., de Paula Corrêa, M., 2016. Hotspots of black carbon and PM2.5 in an urban area and relationships to traffic characteristics. Environ. Pollut. 218, 475–486. https://doi.org/10.1016/j.envpol.2016.07.027. https://www.sciencedirect.com/science/article/pii/S0269749116305978.

US Environmental Protection Agency, 2022. Inventory of U.S. Greenhouse Gas Emissions and Sinks: 1990-2010. EPA, Washington, D.C. https://www.epa.gov/ghgemissions/inventory-us-greenhouse-gas-emissions-and-sinks.

Valencia, A., Arunachalam, S., Isakov, V., Naess, B., Serre, M., 2021. Improving emissions inputs via mobile measurements to estimate fine-scale Black Carbon monthly concentrations through geostatistical space-time data fusion. Sci. Total Environ. 793, 148378 https://doi.org/10.1016/j.scitotenv.2021.148378. https://www.sciencedirect.com/science/article/pii/S0048969721034495.

Van den Bossche, J., Peters, J., Verwaeren, J., Botteldooren, D., Theunis, J., De Baets, B., 2015. Mobile monitoring for mapping spatial variation in urban air quality: development and validation of a methodology based on an extensive dataset. Atmos. Environ. 105, 148–161. https://doi.org/10.1016/j.atmosenv.2015.01.017. https://www.sciencedirect.com/science/article/pii/S1352231015000254.

von Fischer, J.C., Cooley, D., Chamberlain, S., Gaylord, A., Griebenow, C.J., Hamburg, S. P., Salo, J., Schumacher, R., Theobald, D., Ham, J., 2017. Rapid, vehicle-based identification of location and magnitude of urban natural gas pipeline leaks. Environ. Sci. Technol. 51, 4091–4099. https://doi.org/10.1021/acs.est.6b06095.

Weller, Z.D., Hamburg, S.P., von Fischer, J.C., 2020. A national estimate of methane leakage from pipeline mains in natural gas local distribution systems. Environ. Sci. Technol. 54, 8958–8967. https://doi.org/10.1021/acs.est.0c00437.